Spatial Dynamics of Steady Flames 1. Phase Space Structure and the Dynamics of Individual Trajectories

Michael J. Davis*,† and Alison S. Tomlin‡

Chemical Sciences and Engineering Division, Building 200, Argonne National Laboratory, Argonne, Illinois 60439, and School of Process, Environmental, and Materials Engineering, University of Leeds, Leeds, United Kingdom

Received: February 15, 2008; Revised Manuscript Received: April 24, 2008

The spatial dynamics of steady, one-dimensional premixed H_2/O_2 flames are studied. The emphasis in this Article is the geometry of the phase space of the dynamical system describing the steady flames. It is shown that steady flames are described by trajectories on the stable manifolds of saddle fixed points. The saddle fixed points correspond to equilibrium points of time-dependent chemical-kinetic systems that are adiabatic and isobaric and whose constant enthalpy matches the asymptotic enthalpy of the flames. The dimensions of the stable manifolds match the dimensions of the chemical-kinetic systems under most conditions, although the dynamics on them are different. It is further shown that the stable manifolds have low-dimensional attractive submanifolds near the saddlepoint. An algorithm for generating trajectories over the spatial domain of these flames is proposed, and it is used to study individual trajectories and trajectory ensembles, whose collective behavior suggests that there are low-dimensional submanifolds away from the saddlepoint.

I. Introduction

The accurate modeling of reactive flows requires the description of the interplay of chemistry and transport.[1] Steady, one-dimensional flames are among the simplest versions of such systems, and there are many examples of studies of them.[2] Of particular interest in this Article is the approach developed by Hirschfelder and Curtiss[3] as well as Dixon-Lewis,[4] because it studied steady flames as dynamical systems within a multispecies, multicomponent transport model. This formulation is a natural starting point for the study of flames within a dynamical-systems context and is used in this Article and the one that follows.[5]

The modeling of chemically reacting flows is computationally intensive,[1] and so it has been of general interest to develop rational methods for reducing the complexity of these systems, reviewed in several papers.[6] The development of these methods continues, with many new ideas and extensions of old ideas developed in the last several years.[7–26] Many of these methods involve dynamical-systems analysis.[27] These methods provide a natural way of studying complex, homogeneous chemical kinetics, because the systems they describe are closed and eventually approach an equilibrium point. When there is a separation of time scales, the approach to equilibrium occurs on surfaces of lower dimension, so-called low-dimensional manifolds. These low-dimensional manifolds are global, nonlinear realizations of the linear manifolds that are well defined at equilibrium[17,27] and are more mathematically rigorous than steady-state approximations.[28]

The purpose of this Article and the one that follows[5] is to understand how transport processes affect low-dimensional manifolds, something that has spurred a good deal of recent interest.[12,14,15,19–21,23,24,26,29] The introduction of ref 23 provides a recent review of the literature on reduction including a detailed discussion for systems with reaction and transport. The studies here and in ref 5 are most similar to those in ref 20 because they focus on the dynamics of steady flames in an extended space as outlined in refs 3 and 4. This paper and ref 5 extend that analysis by investigating in detail the dynamics of these systems in the spatial domain, with the following Article[5] including more accurate techniques for generating two-dimensional manifolds. Two-dimensional manifolds describe important features of the flame process.

This work, along with ref 20, is an extension to unstable systems of the methods developed for stable systems. The low-dimensional manifolds studied here are submanifolds of stable manifolds of an inherently unstable system.[30] Extra care is necessary in investigating the dynamics of these systems because of their instability. It is this instability that led to the development of computer codes[30,31] to solve the steady flame problem as a set of coupled second-order differential equations using boundary value techniques rather than the dynamical-systems approach of Hirschfelder−Curtiss.[3]

Although the dynamical-systems approach is challenging due to the instability of the systems, it provides a more direct connection to earlier work on reduction techniques whose bases are dynamical in nature. For example, steady flames can be studied as initial-value problems with the dependent variable being space rather than time as it is in homogeneous chemical kinetics. Therefore, it is not necessary to be concerned with the boundary conditions and how they affect the generation of manifolds, something that has been criticized in the past.[29]

The outline of this Article is as follows. Section II gives some background information, including a brief overview of adiabatic, isobaric chemical kinetics and an overview of the calculation of premixed one-dimensional flames with some results from the Chemkin-II program premix.[31] In section III, the approach of Hirschfelder−Curtiss[3] and Dixon-Lewis[4] is presented and used to study the flames as dynamical systems. In this section, it is shown how the flames appear to approach low-dimensional manifolds in the species phase space, and some comparisons

* Corresponding author. E-mail: davis@tcg.anl.gov.
† Argonne National Laboratory.
‡ University of Leeds.

10.1021/jp801367x CCC: $40.75
Published on Web 08/07/2008

are made to the chemical-kinetic case. It is also shown in section III how the boundary value problem (BVP) of ref 31 converges to the initial value problem (IVP) studied here.

The material developed in sections II and III leads to a systematic study of the dynamics of the flames, first near the saddlepoint in section IV, where a detailed analysis of the asymptotic properties of the flames is studied numerically and compared to the asymptotic dynamics of the chemical-kinetic problem. The local analysis of section IV leads to the global analysis of the dynamics in section V, where trajectories are studied, and it is shown that the trajectories appear to approach low-dimensional manifolds. Section VI has further discussion and conclusions. The Article that follows[5] takes the information developed here and extends it to the calculation of low-dimensional manifolds and compares these manifolds to those generated from homogeneous chemical kinetics. Subsequent papers will study aspects of the problems presented here and in ref 5 from a more fundamental perspective.[32]

II. Background

A. Adiabatic Isobaric Chemical Kinetics. One of the purposes of this Article and the subsequent one[5] is to contrast the behavior of the chemical-kinetic systems without transport and the spatial dynamics of flames, both studied in phase space. This subsection provides information concerning the dynamics of adiabatic, isobaric chemical-kinetic systems that will be contrasted below with features of the flame system, starting with section III.A. This information will be most important in the following Article,[5] where direct comparisons are made.

We study here the H_2/O_2 system as described in ref 33. There are 10 species in this system: H_2, O_2, H, O, OH, HO_2, H_2O_2, H_2O, Ar, and He. With temperature, the total dimension of the system is 11.

The chemical kinetics are studied under constant pressure conditions. This fixes the enthalpy as a constant throughout the reaction, giving rise to adiabatic, isobaric conditions. The equations of motion for the chemical species are:

$$\frac{\mathrm{d}Y_k}{\mathrm{d}t} = \frac{W_k\dot{\omega}_k}{\rho} \tag{2.1a}$$

The time development of the temperature is:

$$\frac{\mathrm{d}T}{\mathrm{d}t} = -\frac{1}{\rho c_\mathrm{p}}\sum_k W_k\dot{\omega}_k h_k \tag{2.1b}$$

The Y_k's are mass fractions, W_k's are molecular weights, $\dot{\omega}_k$'s are the chemical production rates (law of mass action), ρ is the density of the gas mixture, c_p is the constant pressure heat capacity, and h_k is the specific enthalpy of a species.

It is assumed that the system obeys the ideal gas law. This allows the Y_k's to be converted to concentrations and densities. In addition to enthalpy, there are four constants of motion:

$$c_\mathrm{O} = 2\frac{Y_{\mathrm{O}_2}}{W_{\mathrm{O}_2}} + \frac{Y_\mathrm{O}}{W_\mathrm{O}} + \frac{Y_\mathrm{OH}}{W_\mathrm{OH}} + 2\frac{Y_{\mathrm{HO}_2}}{W_{\mathrm{HO}_2}} + 2\frac{Y_{\mathrm{H}_2\mathrm{O}_2}}{W_{\mathrm{H}_2\mathrm{O}_2}} + \frac{Y_{\mathrm{H}_2\mathrm{O}}}{W_{\mathrm{H}_2\mathrm{O}}} \tag{2.2a}$$

$$c_\mathrm{Ar} = Y_\mathrm{Ar} \tag{2.2b}$$

$$c_\mathrm{He} = Y_\mathrm{He} = 0 \tag{2.2c}$$

$$\sum_k Y_k = 1 \tag{2.2d}$$

In addition to the O-elemental constant in eq 2.2a, there is a similar constant for the H-element, but it is redundant with the rest of the constants. So along with the constant enthalpy there are five constants of motion and the system is six dimensional. In all calculations presented in this Article, five species are followed (O, OH, HO_2, H_2O_2, H_2O) as well as temperature by integrating eqs 2.1a and 2.1b, and the other five species (H_2, O_2, H, Ar, He) are calculated using the constants. The constants are fixed at the beginning of the trajectory.

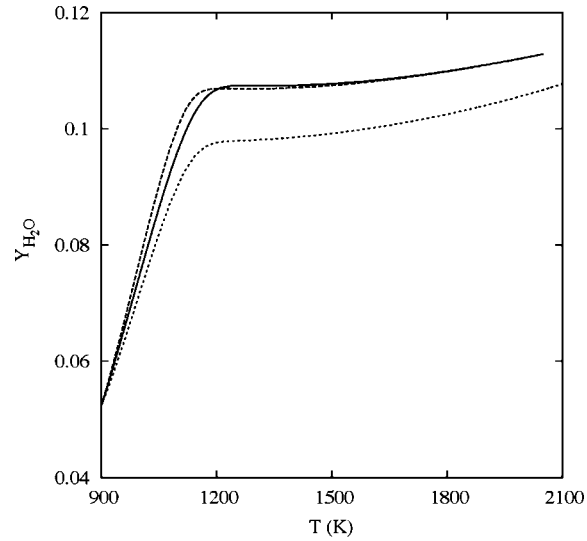

Figure 1. Two trajectories for adiabatic, isobaric chemical-kinetic systems (dashed lines) are plotted along with the flame of Figure 2 (solid line). The chemical-kinetic systems have the same initial conditions in the six independent degrees of freedom as the flame has at $T = 900$ K. The trajectory plotted with longer dashed lines has the same elemental constants and enthalpy as the flame does asymptotically. The trajectory plotted with shorter dashed lines has the same constants and enthalpy as the flame does at 900 K at the beginning of its trajectory.

Two trajectories for the chemical-kinetic systems are propagated and plotted in Figure 1. These trajectories have the same initial conditions in the six propagated variables, Y_O, Y_OH, Y_{HO_2}, $Y_{\mathrm{H}_2\mathrm{O}_2}$, $Y_{\mathrm{H}_2\mathrm{O}}$, and T, but differ in the value of the constants and the enthalpy as described in the figure caption. As expected, the final temperature of the higher enthalpy trajectory is greater than that of the lower enthalpy trajectory.

Figure 1 demonstrates that a typical flame experiences a range of chemical-kinetic behavior. Although Figure 1 concentrates on two variables, temperature and the mass fraction of H_2O, any projection shows a range, although the shapes of the curves and the relative ranges vary with the projections. The rest of the Article and ref 5 often use the same projection, along with projections in the O-atom variable. The temperature is chosen because much of the phase space structure is monotonic in this variable. The same is generally true for H_2O, which is principally chosen because it is the main final product of the H_2/O_2 system. The O-atom variables are generally used because the phase space structure shows curvature in those variables and because the values of the variables are small, so that they test the accuracy of the methods used in ref 5. In addition, the difference between the chemical kinetics and the flames is most pronounced for the O-atom.

The equilibrium configuration of a chemical-kinetic system is found from solving the following set of nonlinear algebraic equations:

$$0 = \frac{W_k \dot{\omega}_k}{\rho} \tag{2.3a}$$

$$0 = \sum_k W_k \dot{\omega}_k h_k \tag{2.3b}$$

at fixed values of the constants from eq 2.2a, which means that only five of the mass fractions and temperature are used to solve eqs 2.3a and 2.3b. Associated with the equilibrium point are a set of eigenvalues and eigenvectors that describe the dynamics near equilibrium. These are found from diagonalization of the Jacobian matrix:

$$J_{mk} = \frac{\partial F_m}{\partial y_k} \tag{2.4}$$

where the F_m's refer to the right-hand sides of eqs 2.1a and 2.1b, and the y_k's refer to the Y_k's and T. Because of the constants, the Jacobian matrix is 6×6, and because the equilibrium defined in eqs 2.3a and 2.3b is stable all eigenvalues are negative. Near equilibrium a chemical-kinetic system is described by the eigenvalues and eigenvectors of the Jacobian.[27] If the eigenvalue spectrum of the matrix **J** has large gaps in it, trajectories will approach equilibrium along the directions of the eigenvectors whose eigenvalues are least negative, with the final approach along a single eigenvector, the one whose eigenvalue is least negative. The low-dimensional manifolds studied in this paper are the global, nonlinear extension of these manifolds. Reference 27 has mathematical discussions of these points. Applications and further, less technical discussions can be found, for example, in ref 17.

B. Flames. The Chemkin program premix[31] calculates the structure of one-dimensional steady flames. Results are generated by solving the following version of the steady-state conservation equations:

$$\frac{dG_k}{dx} - \frac{AW_k \dot{\omega}_k}{\dot{M}} = 0 \tag{2.5a}$$

$$\frac{d}{dx}\left(\frac{\lambda A}{\dot{M}}\frac{dT}{dx}\right) - \frac{d}{dx}\left(\sum G_k h_k\right) = 0 \tag{2.5b}$$

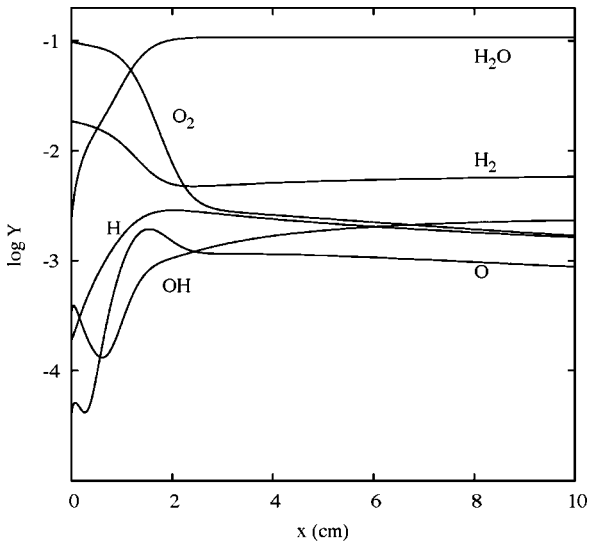

Figure 2. Species profiles of a flame calculated with the Chemkin program premix are shown as a function of distance from the burner in centimeters. The log of the mass fractions are plotted versus this distance.

$$G_k = Y_k + \frac{\rho A V_k Y_k}{\dot{M}} \tag{2.5c}$$

Y_k, $\dot{\omega}_k$ ρ, and W_k were defined for eq 2.1a. The other variables and constants appearing in eqs 2.5a,b are the G_k's, the mass flux fractions, $\dot{M}$, the mass flow rate, V_k, the diffusion velocity, and λ, the thermal conductivity. The area, A, is set to one in all calculations, so the calculations are equivalent to studying fluxes. These equations are coupled with the continuity equation and the ideal gas law. The flames are run under constant pressure conditions. Although there is only a first derivative visible in eq 2.5a, it is a second-order equation, because the diffusion velocity, V_k, has a first derivative term in it. The mass flux fraction describes the fraction of mass flux for a given species. The diffusion velocity describes the velocity of a species relative to the overall velocity of the flow. Good descriptions of the diffusion velocity and mass flux fractions can be found, for example, in ref 3. The present study uses multicomponent transport, and the form of the diffusion velocity is complicated.[31] In the formulation described in section III.A, it does not need to be explicitly calculated. Asymptotically the diffusion velocities go to zero, and therefore asymptotically the mass fractions and mass flux fractions are equal.

Premix uses two methods to solve the system in eqs 2.5a−c. The preferred, default, method is a Newton−Raphson approach that solves a set of nonlinear equations formed by the spatial discretization of the derivative terms. Sophisticated adapted gridding is used.[31] Under some conditions, this procedure does not converge, and a pseudo-time stepping approach to the full transient problem is undertaken.[31] This latter procedure is more stable, but considerably more time-consuming.

Premix solves these equations as a boundary value problem. The mass flux fractions, which are labeled here as G's above and as "ε" in the premix documentation,[31] are read in at the burner end. For a typical flame, only H_2, O_2, Ar, and possibly He are set to nonzero mass flux fractions at the burner. At large values of x, the gradients of the mass fractions, as well as the temperature gradient, are set to zero. Equations 2.5a and 2.5b are solved with the constraints imposed by eqs 2.2b and 2.2c. An example from a typical run of the code for the H_2/O_2 system is shown in Figure 2. These calculations were run to very large values of x (30 m), but only the first 10 cm are shown. Because the premix code does not include radiative loss,[1] the asymptotic value of temperature is not room temperature. The calculation of the flame in Figure 2 was undertaken under conditions of multicomponent transport and thermal diffusion was ignored in the calculations.[31] It is possible to input different mixtures at the burner, changing the shapes of the curves in Figure 2, especially over the first 2 cm, where much of the interesting transient behavior occurs. No plots like this are presented in this Article, but Figure 6 shows calculations of different mixtures at the burner using the premix code, with these plotted in phase space for specific 2-D and 3-D projections.

The flame of Figure 2 is also plotted in Figure 1 (solid line) and is compared there to chemical-kinetic trajectories. This comparison demonstrates the range of chemical-kinetic behavior in the flame, as well as the range of constants and enthalpy in the flame. A more complete view of these changes is provided in Figure 3. The top panel of Figure 3 shows the temperature, and the bottom three panels track the chemical-kinetic constants in the flame. The second panel shows the mass fraction of Ar, the third panel the enthalpy of the mixture, and the bottom panel the O-elemental constant. The enthalpy changes the most of all of the quantities that are constant for the chemical kinetics, and this is a common feature of the flames we have studied.

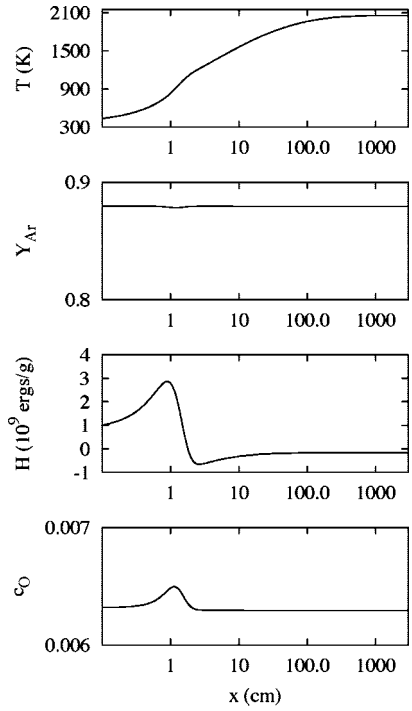

Figure 3. The temperature changes along the flame are plotted along with the quantities that are constant for the adiabatic, isobaric kinetics. The top panel shows the temperature and panels 2−4 the Ar mass fraction, the enthalpy of the mixture, and the elemental O constant (eq 2.2a).

Although the chemical-kinetic constants are not strictly conserved in the flame, Figure 3 suggests that the strongest difference between the flame and chemical-kinetic systems occurs near 1 cm. Although the information contained in Figure 3 is not used in this Article, it is important in the following Article,[5] where more detailed comparisons are made between the dynamics of the flames and chemical-kinetic systems.

III. Steady Flames as Dynamical Systems

A. Hirschfelder−Curtiss/Dixon-Lewis Formulation. The work of Hirschfelder and Curtiss[3] and Dixon-Lewis[4] provides an alternative formulation to eqs 2.5a−2.5c. The flame is cast as a dynamical system and is solved as an initial value problem. In the Hirschfelder−Curtiss/Dixon-Lewis approach, the following set of equations is solved:

$$\frac{dG_k}{dx} = \frac{W_k\dot{\omega}_k}{\dot{M}} \tag{3.1a}$$

$$\frac{dX_k}{dx} = \frac{\dot{M}}{n}\sum_j \frac{(X_kW_kG_j - X_jW_jG_k)}{W_kW_jD_{kj}} \tag{3.1b}$$

$$\frac{dT}{dx} = \frac{\dot{M}}{\lambda}\left(\sum G_kh_k - \bar{h}_\infty\right), h_k = \frac{H_k}{W_k} \tag{3.1c}$$

All of the variables in these equations have been defined above, except for the mixture-averaged asymptotic value of the enthalpy, $\bar{h}_\infty$, and X_k, which is mole fraction. In eq 3.1c, H_k refers to the standard enthalpy of formation. There are two other equations in addition to eqs 3.1a−c that need to be used to fully define the problem, and these are the continuity equation (conservation of mass) and an equation of state. Typically the ideal gas law is used for the equation of state, and that is what is used in Premix and in this Article. It is again assumed that the flow is low speed and that pressure is constant. In the discussion that follows, the following shorthand is used to refer to all of the differential equations, and once again, as in eq 2.4, the Jacobian of the system:

$$\frac{dy_m}{dx} = F_m \tag{3.1d}$$

$$J_{mk} = \frac{\partial F_m}{\partial y_k} \tag{3.1e}$$

where the y's refer to the G's, X's, and T. As described in eqs 3.1a,b, an H_2/O_2 steady flame is a dynamical system whose dimension is 21.

The flame system possesses constants of motion that are:

$$d_O = 2\frac{G_{O_2}}{W_{O_2}} + \frac{G_O}{W_O} + \frac{G_{OH}}{W_{OH}} + 2\frac{G_{HO_2}}{W_{HO_2}} + 2\frac{G_{H_2O_2}}{W_{H_2O_2}} + \frac{G_{H_2O}}{W_{H_2O}} \tag{3.2a}$$

$$d_{Ar} = G_{Ar} \tag{3.2b}$$

$$d_{He} = G_{He} = 0 \tag{3.2c}$$

$$\sum_k X_k = 1 \tag{3.2d}$$

$$\sum_k G_k = 1 \tag{3.2e}$$

Once again, there is a constant associated with the H-element, similar to eq 3.2a, but it is redundant with the constants given. The enthalpy of the mixture is no longer constant, as it was for chemical-kinetic systems in eqs 2.1a and 2.2a. The constant enthalpy has been replaced by an asymptotic enthalpy in eq 3.1c. The mole fractions in eq 3.1b can be converted to concentrations and densities via the ideal gas law and the temperature defined in eq 3.1c. Because there are five constants, the final dimension of the system is 16. It should be noted that the constants defined in eq 3.2a have the same form as those in eq 2.2a, but the c's in eq 2.2a are not constant in the flame. Only under conditions where the diffusion velocities are zero are the c's constant in the flame, which is what happens asymptotically.

The dynamical system defined in eqs 3.1a−c is unstable. The fixed point defined by the conditions:

$$0 = \frac{W_k\dot{\omega}_k}{\dot{M}} \tag{3.3a}$$

$$0 = \frac{\dot{M}}{n}\sum_j \frac{(X_iW_iG_j - X_jW_jG_i)}{W_iW_jD_{ij}} \tag{3.3b}$$

$$0 = \frac{\dot{M}}{\lambda}\left(\sum G_kh_k - \bar{h}_\infty\right) \tag{3.3c}$$

is a saddlepoint. Equation 3.3a defines a chemical equilibrium, as it is a solution of eq 2.3a. However, the diffusion equations (eq 3.3b) make the fixed point unstable, as can be observed numerically by generating the eigenvalues of the Jacobian in eq 3.1e. Although the dynamical system is unstable, associated with a saddle fixed point is a stable manifold. The stable manifold of the fixed point is defined:[27,34]

$$W^s(\mathbf{y}_0) := \{\mathbf{y} \in \mathbf{R}^n | \lim_{t\to\infty} \varphi^t(\mathbf{y}) = \mathbf{y}_0\} \tag{3.4}$$

In eq 3.4, $\mathbf{y_0}$ refers to the fixed point. In words, eq 3.4 states that the stable manifold (W^s) is the set of all vectors that approach the fixed point as t or x (the independent variable)

goes to infinity. For adiabatic, isobaric chemical kinetics, all trajectories in the physical space go to the equilibrium point, and thus the stable manifold has the same dimension as the physical space, six. The physical space is the portion of phase space where all of the variables have physical values. For example, all concentrations are greater than zero in the physical space. It is also possible for such systems to have stable manifolds of this dimension that extend beyond the physical space, and ref 17 has examples. For unstable systems, such as the flames studied here, the stable manifold is a subset of the available space, and its dimension will be calculated below for several systems.

Equations 3.1a−3.4 define the conditions under which there are steady flames. Equations 3.1a−c describe the dynamics. Equations 3.2a−c describe constraints on the system, and eqs 3.3a−3.4 describe the conditions under which the system is stable. Equations 3.1a−3.4 thus show that steady flames are trajectories on the stable manifold of a saddle fixed point.

Equations 3.1a−c describe a dynamical system with physical and unphysical solutions, like many differential equations. The physical solutions are asymptotically stable, and the unphysical ones blow up. The last point in the previous paragraph describes the geometrical realization of this feature of the differential equations, and eq 3.4 puts it in mathematical terms.

We end the discussion of the dynamical system defined in eqs 3.1a−3.4 by generating a similar set of equations for a simpler system as a way of explaining the coordinate system. The equations result from adding advection to one of the systems studied in ref 24 (a), which is revisited in section III.D. In addition, the diffusivity is assumed to have a spatial dependence, something which is true in the flame system. Starting with the following advection-diffusion-reaction evolution equation for one of the species in an isomerization reaction:

$$\frac{\partial y_1}{\partial t} = -k_1 y_1 + k_2 y_2 + v\frac{\partial y_1}{\partial x} + \frac{\partial}{\partial x}\left(D\frac{\partial y_1}{\partial x}\right) \qquad (3.5a)$$

the steady state equation is defined:

$$0 = -k_1 y_1 + k_2 y_2 + v\frac{\mathrm{d}y_1}{\mathrm{d}x} + \frac{\mathrm{d}}{\mathrm{d}x}\left(D\frac{\mathrm{d}y_1}{\mathrm{d}x}\right) \qquad (3.5b)$$

where v is a constant flow velocity. Moving the derivative terms to the left-hand side and manipulating eq 3.5b gives the following:

$$\frac{\mathrm{d}}{\mathrm{d}x}\left(y_1 + \frac{D}{v}\frac{\mathrm{d}y_1}{\mathrm{d}x}\right) = \frac{1}{v}(k_1 y_1 - k_2 y_2) \qquad (3.5c)$$

$$\frac{\mathrm{d}G_1}{\mathrm{d}x} = \frac{1}{v}(k_1 y_1 - k_2 y_2),\ G_1 \equiv y_1 + \frac{D}{v}\frac{\mathrm{d}y_1}{\mathrm{d}x} \qquad (3.5d)$$

$$\frac{\mathrm{d}y_1}{\mathrm{d}x} = \frac{v}{D}(G_1 - y_1) \qquad (3.5e)$$

In addition, the diffusion velocity can be defined in a straightforward manner:

$$V_1 = D\frac{\mathrm{d}y_1}{\mathrm{d}x} \qquad (3.5f)$$

Equations 3.5d−3.5e describe the dynamics for one species, and there is another set for the other species.

Equations 3.5d and 3.5e are analogous to eqs 3.1a and 3.1b. They define two of four equations necessary to study a steady advection-diffusion-reaction equation for an isomerization reaction as a dynamical system. It is also possible to find the saddlepoint of this system and confirm that it is in fact a saddlepoint. The saddlepoint is defined by:

$$0 = \frac{1}{v}(k_1 y_1 - k_2 y_2) \qquad (3.5g)$$

$$0 = \frac{v}{D}(G_1 - y_1) \qquad (3.5h)$$

Under most conditions, the eigenvalues of the Jacobian for the full four-dimensional system will have two negative eigenvalues and two positive eigenvalues at this point, indicating that it is a saddlepoint. Equation 3.5h indicates that at the saddlepoint the G's and y's are equal. As noted above, for the flame system the G's and Y's (mass fractions in that case) are equal at the saddlepoint.

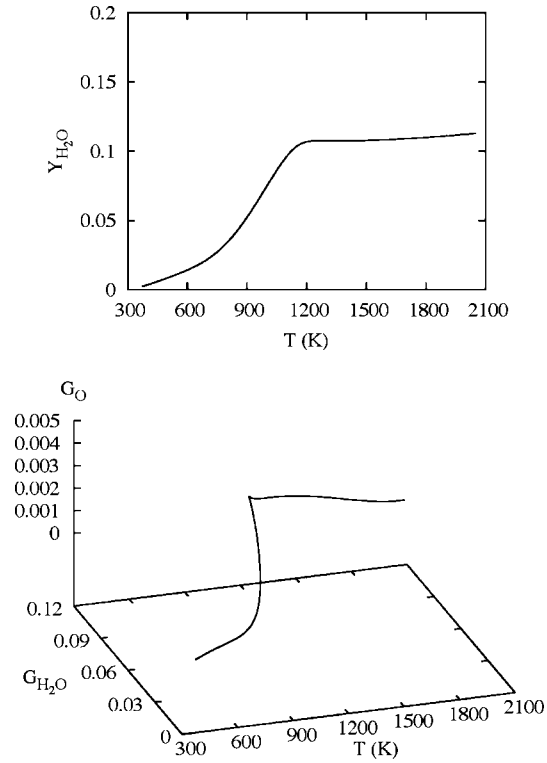

Figure 4. The flame of Figures 2 and 3 is plotted out to large spatial extent and in a space of the species and temperature. A two-dimensional projection is shown in the top panel, and a three-dimensional projection is shown in the bottom panel.

In preparation for the dynamical system analysis described in the rest of the Article and in ref 5 where low-dimensional manifolds are investigated, it is useful to first study the dynamics in phase space as it moves toward the saddlepoint. The results of such a calculation for the Premix program are presented in Figure 4 where the calculation was carried out to 30 m. The top panel shows a two-dimensional projection onto the space of the temperature and H_2O mass fraction, and the bottom panel of Figure 4 shows a three-dimensional projection using temperature and the mass flux fractions of H_2O and O-atom. This panel demonstrates that there are sudden changes in gradient in a couple of places. Such changes are generally indicative of low-dimensional manifolds, whose presence is demonstrated in ref 5.

B. Dynamics of a Chemical-Kinetic System: Approach to Low-Dimensional Manifolds. A common feature of chemical-kinetic systems is that they approach equilibrium via low-dimensional manifolds due to a separation of time scales. This behavior is well-known for the H_2/O_2 system,[17] and a random

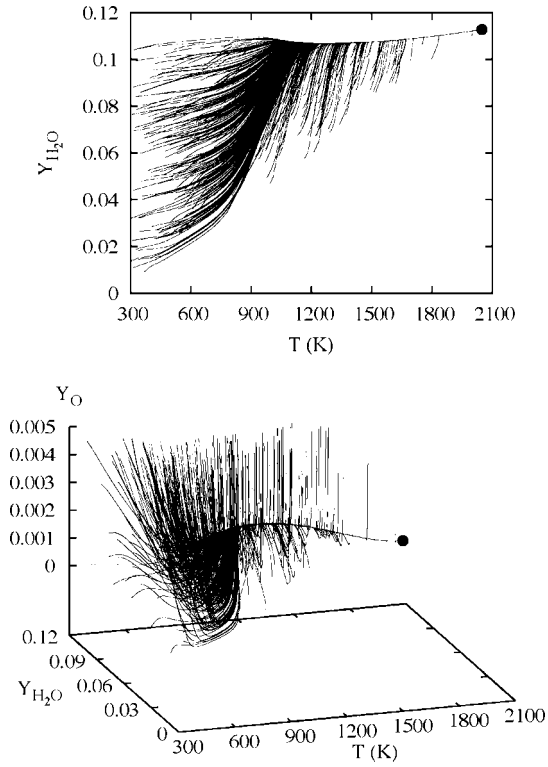

Figure 5. A set of 400 randomly selected trajectories were run in a chemical-kinetic system and plotted as a two-dimensional projection in the top panel and a three-dimensional projection in the bottom. The equilibrium point is plotted as a large dot. The top panel shows strong evidence for a one-dimensional manifold, and the bottom panel shows evidence for a two-dimensional manifold.

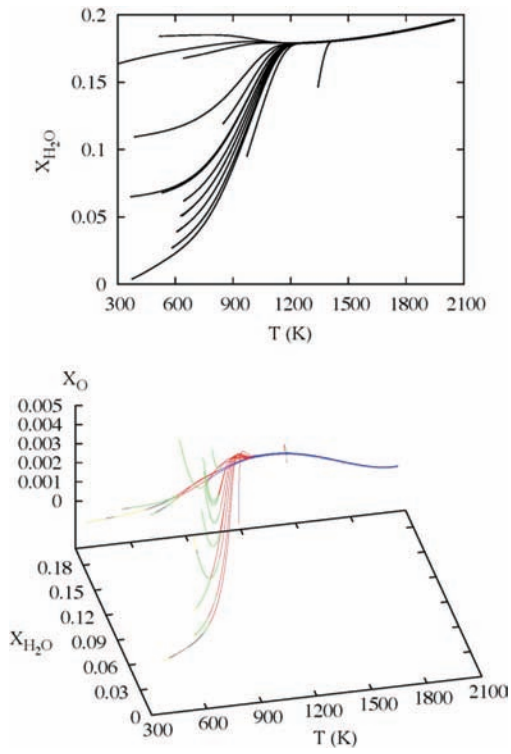

Figure 6. A series of 16 flames were generated from the Chemkin program Premix and plotted with a two-dimensional projection in the top panel and a three-dimensional projection in the bottom panel. These calculations were chosen to have approximately the same asymptote. The top panel makes it clear that there is a one-dimensional manifold for the flame, and the bottom panel suggests there is a two-dimensional manifold, but the data are rather sparse. Further evidence of the dimensionality is provided in the panel by an estimate of the dimensionality: $n = 1$ (blue), $n = 2$ (red), $n = 3$ (green), $n = 4$ (black), and $n = 5$ (yellow).

sample of trajectories for the chemical-kinetic system of section II.A shows such behavior. The top panel of Figure 5 shows a two-dimensional projection of a random sample of 400 trajectories. These are propagated for a system with an enthalpy equal to the asymptotic enthalpy of the flame generated with the method of section V, -1.755×10^8 ergs/g. In addition, the two elemental constants are set to the asymptotic elemental constants of the same flame (the c's in eqs 2.2a and 2.2b), $c_O = 0.0063$, $c_{Ar} = 0.88$. It is clear from this panel that trajectories approach a one-dimensional manifold at $T \cong 1200$ K and $Y_{H_2O} > 0.1$.

The bottom panel extends the analysis by showing a three-dimensional projection. It appears that the sample of trajectories approaches a two-dimensional surface for $T > 850$ K, $Y_{H_2O} > 0.06$, and Y_O small. Reference 5 will present pictures of the one- and two-dimensional manifolds.

As noted above in the discussion of Figure 1, trajectory plots presented in this Article and in ref 5 are usually drawn with projections involving the temperature, H_2O, and O-atom variables, for reasons stated there. Because of the monotone behavior of the temperature and the near-monotone behavior of the H_2O variables (mass fractions, mole fractions, or mass flux fractions), it is more straightforward to observe the collapse of trajectories to manifolds in plots such as the ones shown in Figure 5 and later plots in this Article and ref 5.

C. Flame Dynamics: Approach to Low-Dimensional Manifolds. To demonstrate that flames from the Chemkin program Premix have a behavior similar to that of chemical-kinetic systems, several flames were generated from the code and presented in Figure 6. The initial values of the species at the burner were adjusted so that the flames would have the same spatial asymptotes. This procedure was generally successful, but the line is extra thick because the asymptotes are slightly different.

In the top panel of Figure 6, the results from 16 flame calculations are plotted in a manner similar to that of the chemical-kinetic system in the top panel of Figure 5. These are plotted with the mole fractions, the X's as the variables, as it is the standard set of variables outputed from premix. As will be evident in subsequent portions of the Article, the picture outlined in Figure 6 is apparent in any reasonable set of coordinates, although generally the phase space plots presented in this Article use the mass fractions, the Y_k's, for chemical-kinetic systems and G_k's for the flame systems. These sets of coordinates are preferred, because the chemical-kinetic constants in eq 2.2a are defined for the Y's and the flame constants in eq 3.2a are defined for the G's.

As in Figure 5, Figure 6 demonstrates that there appears to be a one-dimensional manifold at temperatures above approximately 1200 K. The situation is more ambiguous in the bottom panel, where a three-dimensional projection is plotted. Based on the behavior of the trajectories, it appears that a two-dimensional manifold is approached, but the data are sparse.

Further evidence for the dimensionality of the surface on which the flame trajectories move is provided by dimension estimates calculated with the technique of refs 35. The dimension is color coded on the figure, as noted in the caption. The blue portions of the trajectories indicate that the dimension estimate is 1, and the red portions indicate that the dimension

estimate is 2. This is consistent with the more qualitative analysis provided by the changes of gradients in the trajectories.

In subsequent sections of the Article, we will develop the methodology to use the Hirschfelder−Curtiss approach to generate a large number of trajectories for the flame system with the same asymptotes. This will lead to evidence that there are two-dimensional manifolds, which will further be confirmed by finding them in ref 5.

D. Phase Space Structure: Initial Value Problem versus Boundary Value Problem. To understand the phase space structure of the flame, a simpler system is used to demonstrate the general phase space structure of an unstable system. In ref 20 a somewhat more complicated system was studied to establish the nature of the eigenvalue spectrum and the manifolds of the system, which was also linear, like the present case. However, a detailed phase space analysis was not included there. Further analysis of such simple systems, including nonlinear systems, will be presented in a future publication.[32]

Consider the isomerization problem:

$$\mathrm{A} \leftrightarrow \mathrm{B} \tag{3.6}$$

Assuming for convenience that the diffusion constants are equal, the following reaction-diffusion system is defined:

$$\frac{\partial y_1}{\partial t} = -k_1 y_1 + k_2 y_2 + D\frac{\partial^2 y_1}{\partial x^2} \tag{3.7a}$$

$$\frac{\partial y_2}{\partial t} = k_1 y_1 - k_2 y_2 + D\frac{\partial^2 y_2}{\partial x^2} \tag{3.7b}$$

where y_1 and y_2 are densities or concentrations of A and B, respectively, and D is the diffusion constant. The steady solutions of this system are found from:

$$\frac{\mathrm{d}^2 y_1}{\mathrm{d}x^2} = \frac{1}{D}(k_1 y_1 - k_2 y_2) \tag{3.8a}$$

$$\frac{\mathrm{d}^2 y_2}{\mathrm{d}x^2} = \frac{1}{D}(-k_1 y_1 + k_2 y_2) \tag{3.8b}$$

The following linear combination

$$\frac{\mathrm{d}^2(y_1 + y_2)}{\mathrm{d}x^2} \equiv \frac{\mathrm{d}^2(z)}{\mathrm{d}x^2} = 0 \tag{3.9}$$

means that

$$z = \mathrm{d}x + c \tag{3.10a}$$

We are interested in those solutions that are stable and thus restrict to those where:

$$z = c \tag{3.10b}$$

So eq 3.8a can be converted to the following system:

$$\frac{\mathrm{d}^2 y_1}{\mathrm{d}x^2} = \frac{k}{D} y_1 - \frac{k_2 c}{D}, \; k = k_1 + k_2 \tag{3.11}$$

This second-order differential equation can be converted to two first-order equations:

$$\frac{\mathrm{d}y_1}{\mathrm{d}x} = u_1 \tag{3.12a}$$

$$\frac{\mathrm{d}u_1}{\mathrm{d}x} = \frac{k}{D} y_1 - \frac{k_2 c}{D} \tag{3.12b}$$

The system has a fixed point at the equilibrium condition:

$$y_1 = \frac{k_2 c}{k} \tag{3.13a}$$

$$u_1 = 0 \tag{3.13b}$$

The solutions of eqs 3.12a and 3.12b are:

$$y_1 = \frac{1}{2}\left[\left(y_{10} + \sqrt{\frac{D}{k}}u_{10} - \frac{k_2 c}{k}\right)\mathrm{e}^{\sqrt{\frac{k}{D}}x} + \left(y_{10} - \sqrt{\frac{D}{k}}u_{10} - \frac{k_2 c}{k}\right)\mathrm{e}^{-\sqrt{\frac{k}{D}}x}\right] + \frac{k_2 c}{k} \tag{3.14a}$$

$$u_1 = \frac{1}{2}\left[\left(\sqrt{\frac{k}{D}}y_{10} + u_{10} - \sqrt{\frac{k}{D}}\frac{k_2 c}{k}\right)\mathrm{e}^{\sqrt{\frac{k}{D}}x} + \left(-\sqrt{\frac{k}{D}}y_{10} + u_{10} + \sqrt{\frac{k}{D}}\frac{k_2 c}{k}\right)\mathrm{e}^{-\sqrt{\frac{k}{D}}x}\right] \tag{3.14b}$$

The only asymptotically stable solutions of eqs 3.13a and 3.13b are ones where:

$$u_1 = -\sqrt{\frac{k}{D}}y_1 + \sqrt{\frac{k}{D}}\frac{k_2 c}{k} \tag{3.15}$$

(The positive exponentials have zero component.) Therefore, eq 3.15 defines the stable manifold of the saddle fixed point of eqs 3.13a and 3.13b. The unstable manifold (the most unstable direction) is:

$$u_1 = \sqrt{\frac{k}{D}}y_1 - \sqrt{\frac{k}{D}}\frac{k_2 c}{k} \tag{3.16}$$

(The negative exponentials have zero component.)

Equations 3.13a and 3.13b can be used to develop the phase space structure of the system. An alternative way of analyzing the structure is based on recognizing the system is Hamiltonian, with the following Hamiltonian:

$$H = \frac{1}{2}u_1^2 - \frac{k}{2D}y_1^2 + \frac{k_2 c}{D}y_1 \tag{3.17}$$

The unstable and stable manifolds are level curves of the system with the following value:

$$E = \frac{k_2^2 c^2}{2kD} \tag{3.18}$$

These equations can now be used to understand the phase space structure of the system and the role of boundary conditions. Figure 7 shows a series of level curves for the reaction diffusion system in eqs 3.7a and 3.7b with the following set of parameters: $k_1 = 2.0$, $k_2 = 1.0$, and $D = 0.5$, with the constant in eq 3.10b set to 2.0. The stable and unstable manifolds are shown as a set of thick black lines that intersect at the saddlepoint, shown as a solid round dot, and form a separatrix dividing motion that has a turning point ($u_1 = 0$) and motion that does not have a turning point. There are 14 additional level curves; 6 have energies above the separatrix energy and 8 have energies below the separatrix energy.

The following set of boundary conditions will be studied for the reaction−diffusion system:

$$y_{1l}(x = 0) = y_{10}, \; u_{1r}(x = x_r) = 0 \tag{3.19}$$

These were chosen to be similar to those in the Premix code for flames. The "l" refers to the left boundary and "r" refers to the right boundary. This boundary condition restricts allowed steady distributions for the reaction−diffusion system to those that have level curves inside or on the separatrix. The vertical

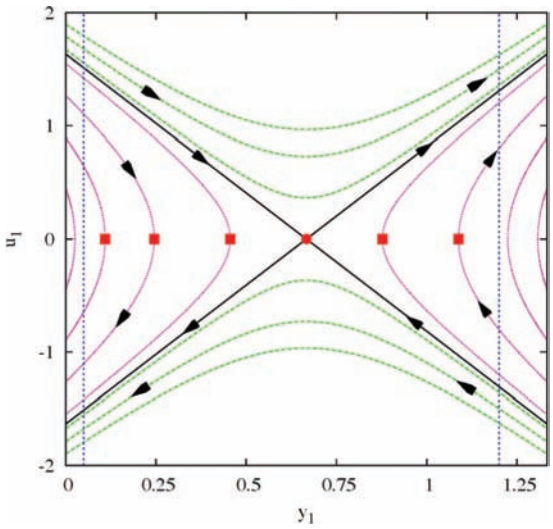

Figure 7. The phase space structure of the steady states of the isomerization reaction−diffusion system is shown here. Several different values of the level curves are shown. The arrows on some of the level curves indicate the direction of the flow. A complete discussion of this figure is in the text.

lines in Figure 7 are at $y_1 = 0.1$ and $y_1 = 1.2$. To satisfy the boundary conditions for these requires that the level curves cross the $u_1 = 0$ line at x_f. There are three level curves shown in Figure 7 that can satisfy the conditions for $y_1 = 0.1$ and two for $y_1 = 1.2$. The solid squares drawn on the $u_1 = 0$ line show the points at which these curves would need to cross at $x = x_f$ to satisfy the right boundary condition.

To impose the second condition in eq 3.19, the left-hand side of eq 3.14b is set to zero, and the following condition results:

$$u_{10} = -\sqrt{\frac{k}{D}}\left(y_{10} - \frac{k_2 c}{k}\right)\frac{e\sqrt{\frac{k}{D}}x_f - e^{-}\sqrt{\frac{k}{D}}x_f}{e\sqrt{\frac{k}{D}}x_f + e^{-}\sqrt{\frac{k}{D}}x_f} \quad (3.20)$$

In the limit of large x_f, the stable manifold is recovered:

$$\lim_{x_f \to \infty} u_{10} = -\sqrt{\frac{k}{D}}y_{10} + \sqrt{\frac{k}{D}}\frac{k_2 c}{k}$$

Therefore, the boundary value problem becomes strictly an initial value problem when the spatial limit is taken to infinity.

The rest of the Article studies the initial value problem presented in section III.A, but it is instructive to first demonstrate how the boundary value problem approaches the initial value problem. The top panel of Figure 8 shows three level curves (dotted lines) near the energy of the stable manifold (solid lines) for the isomerization reaction−diffusion system and is an expansion of part of Figure 7. This panel makes it clear that the solution of the boundary value problem approaches the solution of the initial value problem as the boundary is taken to larger values. The bottom panel of Figure 8 shows similar results for the steady-flame case. There are four steady flames plotted in the bottom panel as calculated from the Premix code. The solid curve was generated out to $x = 1000$ cm and is essentially a two-dimensional projection of the stable manifold. The other curves were generated from the code out to the following boundaries, 10, 50, and 100 cm, and it is clear how they approach the stable manifold and that they differ somewhat from the asymptotic result.

Figure 8 demonstrates that there are small differences between the boundary-value solutions and the initial-value solutions that

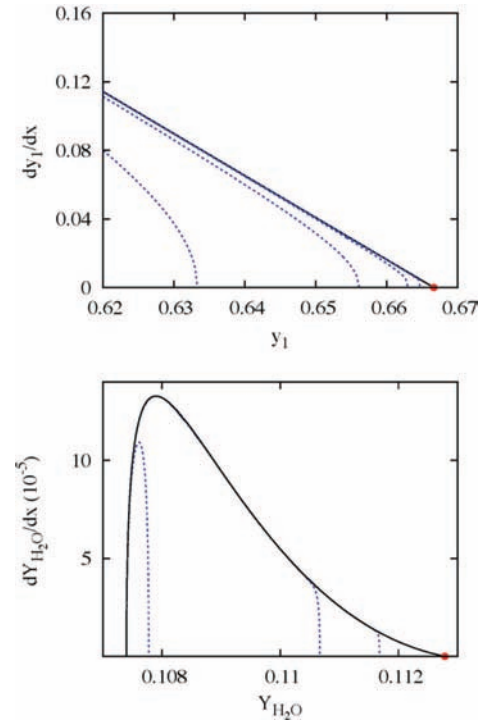

Figure 8. The top panel shows an expanded view of part of Figure 7, showing three level curves (dotted lines) near the separatrix (solid line). The bottom panel shows results for four flames with the boundary-value approach. The dotted lines show flames generated out to 10, 50, and 100 cm. The solid line shows a flame out to 1000 cm, which is essentially the stable manifold for the saddlepoint (solid dot) in the vicinity of the saddlepoint.

are imposed by the boundary conditions. To make accurate comparisons between the flame dynamics and the chemical kinetics without transport, it is essential to avoid differences imposed by the boundary conditions, and such comparisons are presented in the following Article.[5] Figure 8 further demonstrates that flames generated from a boundary-value approach are described by trajectories that do not lie on the stable manifold of a fixed point. Therefore, these trajectories are not directly analogous to trajectories of the chemical-kinetic system whose motion does lie on a stable manifold. On the other hand, flame trajectories generated from an initial-value approach do lie on the stable manifold, and comparisons in phase space between the spatial dynamics of flames and the temporal dynamics of the corresponding chemical-kinetic system are more appropriate within the initial-value approach.

IV. Near Equilibrium Dynamics

A. Phase Space Structure. In section III.D the phase space structure of the reaction−diffusion system could be generated analytically over the whole phase space. It is not possible to do this globally for the flame system, but it is possible to use the Jacobian of the flame system of eq 3.1a to analyze the phase space structure of the flame near the saddlepoint. The purpose of this investigation is to demonstrate the strong instability of the motion away from the stable manifold.

The flame system studied is one that matches the flame of the Premix code that was studied in Figure 2. The calculation of this trajectory is described in section V. It has $d_O = 6.3 \times 10^{-3}$, $d_{Ar} = 0.88$ (eq 3.2a), and $\bar{h}_\infty = -1.755 \times 10^8$ ergs/g. The eigenvalue spectrum of this system at the saddlepoint is: −69.2, −27.1, −22.7, −19.0, −2.3, −0.0061, 0.77, 1.16, 1.20, 3.0, 3.2, 6.3, 23.1, 25.2, 29.7, and 73.4. Because the eigenvalue

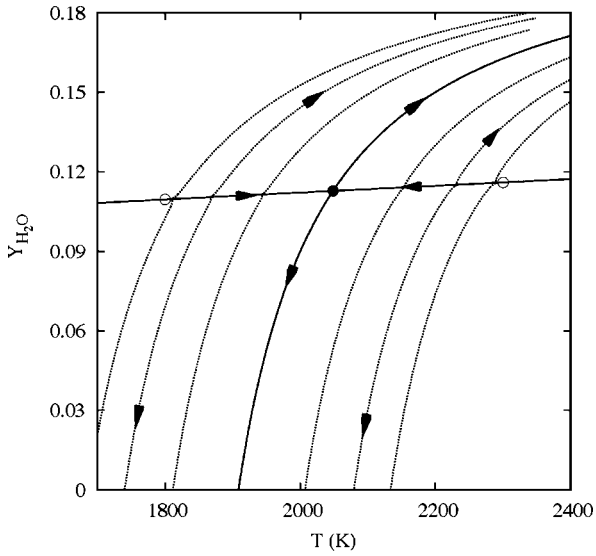

Figure 9. The stable (straight thick, dark line) and unstable manifolds (curved thick line) of the linear system are plotted. These emanate from the saddle point (dot). Twelve trajectories (dotted lines) starting near the stable manifold are also plotted. The arrows drawn on some of the trajectories and on the manifolds indicate the direction of the flow. The text describes the figure in more detail.

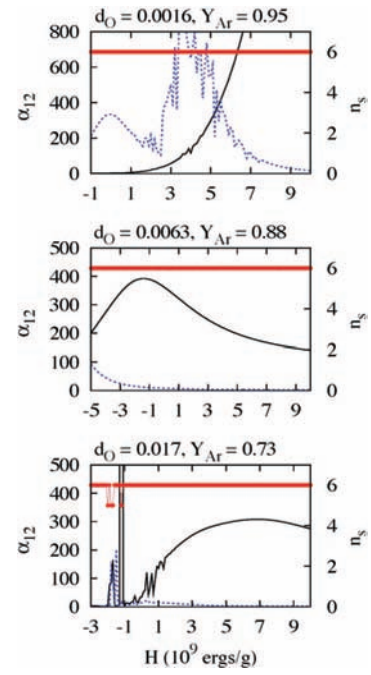

Figure 10. Eigenvalue ratios for three flame systems as a function of asymptotic enthalpy of the mixture are presented for rich flames (top), stoichiometric flames (middle), and lean flames (bottom). Solid lines show α_1, and dashed lines show α_2. The dimension of the stable manifold near the saddle is shown in all panels as a series of dots. Its value is almost always 6, the dimension of the chemical-kinetic space.

spectrum has positive eigenvalues, it is unstable, and because the eigenvalue sum is greater than zero, the system is a repellor.[36] This differs from the isomerization example in the previous section, which was area preserving. To demonstrate the structure of this system and its inherent instability, the subspace of the two eigenvectors associated with the lowest positive eigenvalue (0.77) and least negative eigenvalue (−0.0061) is studied.

The phase space structure of the linear system defined by the eigenvector subspace is shown in Figure 9. The stable manifold is the thick dark line that is nearly linear, and the unstable manifold is the dark curve (the system is linear in the *X*'s and *G*'s, but the transformation from the *X*'s to *Y*'s is nonlinear). There are 12 trajectories propagated in the linear system formed from the eigenvectors and their eigenvalues. They are plotted as dashed curves, and six are started to the left of the saddlepoint (the large solid dot) and six to the right.

The trajectories on the left are started very close to the stable manifold with the starting position at the open circle, with small displacements away from the stable eigenvector along the unstable eigenvector. The ratios of the unstable to stable directions in the figure (from left to right) are: $\pm 1 \times 10^{-5}$, $\pm 1 \times 10^{-20}$, and $\pm 1 \times 10^{-50}$. The trajectories on the right are started at the open circle and are displaced along the unstable direction (from right to left): $\pm 1 \times 10^{-5}$, $\pm 1 \times 10^{-20}$, and $\pm 1 \times 10^{-50}$. These trajectories were chosen to demonstrate the behavior of the system in the vicinity of the saddlepoint, and the displacements along the unstable manifolds had to be extremely small for a trajectory to get past half the distance to the saddlepoint from the initial value before diverging, with only the displacements of $\pm 1 \times 10^{-50}$ on either side of the saddlepoint moving more than half the distance. The sizes of these displacements along the unstable direction demonstrate the strong instability of the system, which can be anticipated by the large ratio in the magnitude of the two eigenvalues of the eigenvector subspace studied (0.77 vs −0.0061).

The degree of instability in Figure 9 demonstrates that it is very hard to use standard integration techniques to generate trajectories for the flame system. Any small displacement from the stable manifold will cause the system to move rapidly away from the stable manifold. It was this instability that led to the development of computer codes based on boundary value techniques.[30,31] Section V presents an alternative means for generating trajectories.

B. The Jacobian and Linear Low-Dimensional Manifolds: Changes with Enthalpy. The Jacobian of the flame system of eq 3.1a can be used to further analyze the dynamics of the system near the saddlepoint. Here, we are interested only in the stable manifold. The local attractivity of the one- and two-dimensional submanifolds on the stable manifold is controlled by the following quantities near equilibrium:

$$\alpha_1 = \frac{\lambda_2^-}{\lambda_1^-} \tag{4.1a}$$

$$\alpha_2 = \frac{\lambda_3^-}{\lambda_2^-} \tag{4.1b}$$

where the superscript "−" indicates that only the negative eigenvalues are studied, and the subscripts "1", "2", and "3" refer to the magnitude of the eigenvalues, with "1" referring to the least negative eigenvalue. When α_1 is large, there is a significant separation of spatial scales for the largest spatial scales and the one-dimensional submanifold of the stable manifold is highly attractive near the saddlepoint. When α_2 is large, there is a strong separation of spatial scales for the second longest spatial scales and the two-dimensional submanifold of the stable manifold is attractive near the saddlepoint.

Figure 10 investigates the ratios defined in eqs 4.1a and 4.1b as a function of the asymptotic enthalpy, $\bar{h}_\infty$. Three different values of the constants d_O and d_{Ar}, as defined in eq 3.2a, are investigated in Figure 10. The panels show α_1 as solid lines and α_2 as dashed lines. The three cases in Figure 10 can be

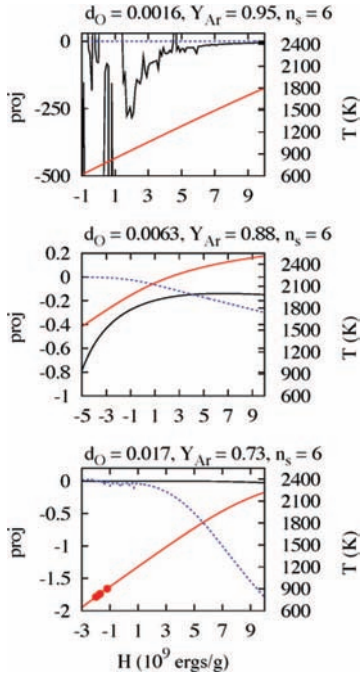

Figure 11. A further analysis of the systems in Figure 10 is presented. The thick red line shows the asymptotic temperature of the systems (right axes). The solid black line shows the ratio of the H-atom mass flux fraction versus H_2O mass flux fraction, and the dotted line shows the analogous quantity for the O-atom.

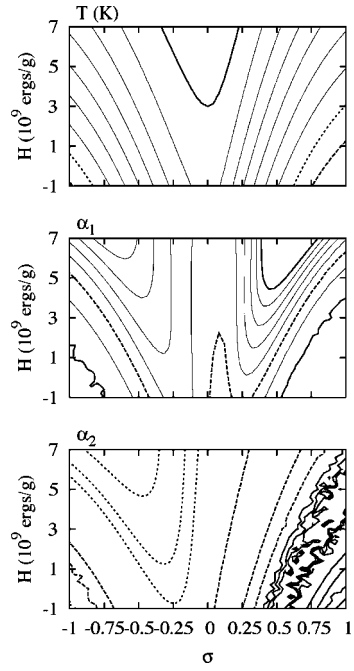

Figure 12. The top panels show contours of the temperature as a function of stoichiometry and enthalpy for the chemical-kinetic systems. The middle panel shows the eigenvalue ratio as defined in eq 4.1a, and the bottom panel shows the eigenvalue ratio defined in eq 4.1b. The bottom two panels show the degree of attractivity of the one- and two-dimensional manifolds. The text has further details.

classified via their stoichiometry as rich flames (top panel), stoichiometric flames (middle), and lean flames (bottom). The panels in Figure 10 also show the dimension of the stable manifold, n_s, as a series of dots, using the right-hand axis. This dimension is equal to the number of negative eigenvalues at the saddlepoint. The panels demonstrate that under almost all conditions the dimension of the manifold is 6, which is the same as the dimension of the chemical-kinetic system of section II.A. Only for four systems is n_s less than 6, and these are flames that experience small temperature rises, reaching asymptotic temperatures of only 900 K (see the bottom panel of Figure 11 for the temperatures). In the rest of this Article, the only systems studied are those whose stable manifolds have dimension 6 and match the dimension of the equivalent chemical kinetic system.

Figure 10 demonstrates that for stoichiometric flames in the middle panel the one-dimensional manifolds are very attractive for all enthalpies, because α_1 is large. The variations of α_1 in the top and bottom panels demonstrate that for the rich and lean cases, one-dimensional manifolds are highly attractive at higher enthalpies, but not necessarily for the lowest enthalpies. For the lean case in the bottom panel, the situation is very complicated at low enthalpies. There are ranges where the one-dimensional manifolds are very attractive and ranges where they are not.

All of the plots in Figure 10 demonstrate that at high enthalpy, two-dimensional manifolds become less attractive as enthalpy gets higher, because α_2 gets smaller. The top two panels demonstrate that at low enthalpy the two-dimensional manifolds are attractive when the enthalpy is less than zero, with α_2 generally greater than 10. Once again, the bottom panel shows that when enthalpy is less than zero the situation gets much more complicated. There are ranges of enthalpy where α_2 gets as high as 100.

Figure 10 also demonstrates that there are ranges of enthalpy where both one- and two-dimensional manifolds are attractive, particularly near $H = 0$. These cases fit the generic relaxation view of Roussel,[10] where there are strongly attractive one- and two-dimensional manifolds.

The complexity observed at low enthalpy in the bottom panel and subsequent plots, most notably in the top panel of Figure 11, the bottom panel of Figure 12, and the middle panel of Figure 13, is interesting. We examined this further and came to the conclusion that the complexity is real and not noise from poor contour resolution or inaccuracy in calculating finite-difference derivatives in generating Jacobian matrices. This phenomenon would be interesting to study in more detail, but we have not done that yet.

Figure 11 extends the analysis of Figure 10. This figure demonstrates the type of analysis that can be done for the flame once the one-dimensional manifold is resolved. The analysis here is done near the saddlepoint as a demonstration of the utility of a geometric analysis of the dynamics of the flame. The solid red line shows the temperature at the saddlepoint (the asymptotic temperature), which, as expected, increases with increasing enthalpy. The four dots on the bottom panel show the four systems in the bottom panel of Figure 10 that have stable manifolds whose dimensions are not 6, and it indicates that these are systems that do not reach a very high temperature. One puzzling aspect of this figure is that these systems do not seem very different from ones near them, but still differ in the dimension of the manifolds. This deserves further attention, but is not investigated any further in this Article.

The rest of the information on Figure 11 refers to the eigenvectors of the two least negative eigenvalues. The solid black lines in the plots show the ratio of the projection of H-atom mass flux fraction of the linear one-dimensional manifold onto the H_2O mass flux fraction and the dashed lines the same ratio for the O-atom. The changes in the one-dimensional manifold thus can be tracked as a function of the stoichiometry and enthalpy. For the rich flame at the top, there is little H-atom produced along the low-dimensional manifold for all enthalpies

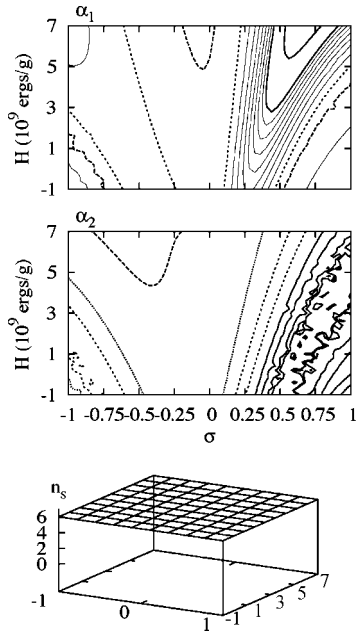

Figure 13. The top two panels describe the eigenvalue ratios for the flame system and are analogous to the bottom two panels of Figure 12. The bottom panel shows the dimension of the stable manifold (the number of negative eigenvalues of the Jacobian), and it is 6 over the range of enthalpies and stoichiometries studied in the figure. This is the same as the dimensions of the chemical-kinetic systems.

and little O-atom produced for high enthalpies. However, at low enthalpies there is a complicated interplay between the H_2O and O-atom productions along the one-dimensional manifolds. For the stoichiometric flames, there are significant amounts of O-atom produced along the one-dimensional manifold as compared to H_2O, with nearly equal amounts at low enthalpies. There is little H-atom produced versus H_2O for the stoichiometric flame at low enthalpies, but a significant fraction at high enthalpies. For the lean flame on the bottom panel, there is almost no O-atom production along the one-dimensional manifold for all enthalpies, but significant amounts of H-atom at high enthalpy.

C. Changes with Enthalpy and Stoichiometry. A broader view of the changes of the manifolds near the equilibria of the chemical-kinetic systems and the saddlepoints of the flame systems is provided in this subsection. Figure 12 presents results for a series of calculations on the chemical-kinetic systems near their equilibrium points, and Figure 13 has a similar series near the saddlepoints of the flame systems. In these calculations, the constants of motion are set by the following conditions:

$$X_{Ar} = 0.63 \tag{4.2a}$$

$$f_s = 2 \tag{4.2b}$$

$$f_{H_2} = \frac{\chi_s f_s}{1 + \chi_s f_s}, \sigma = \log(\chi_s) \tag{4.2c}$$

$$X_{H_2} = f_{H_2}(1 - X_{Ar}) \tag{4.2d}$$

$$X_{O_2} = 1 - X_{Ar} - X_{H_2} \tag{4.2e}$$

$$c_O = d_O = \frac{2Y_{O_2}}{W_{O_2}} \tag{4.2f}$$

$$c_{Ar} = d_{Ar} = Y_{Ar} \tag{4.2g}$$

$$\bar{h}_\infty = \bar{h} = h_i \tag{4.2h}$$

where h_i is the input value of $\bar{h}$, the constant enthalpy of the chemical kinetic system, $\bar{h}_\infty$ refers to the asymptotic enthalpy of the flame, and χ_s is an input parameter describing the stoichiometry. The mass fractions in eqs 4.2f and 4.2g are calculated in the usual manner. For example, the mass fraction of O_2 is calculated from the mole fractions with:

$$Y_{O_2} = \frac{X_{O_2} W_{O_2}}{X_{O_2} W_{O_2} + X_{H_2} W_{H_2} + X_{Ar} W_{Ar}} \tag{4.3}$$

Equations 4.2b and 4.2c indicate that when the flame/reaction system is stoichiometric at the saddle/equilibrium, $\chi_s = 1$ and $\sigma = 0$.

The top panel of Figure 12 shows contours of the temperature as a function of $\bar{h}$ and the stoichiometric parameter σ defined in eqs 4.2b and 4.2c. Temperature contours are from 800 to 2400 K in 200 K increments. The maximum contour at 2400 K is plotted as a thick solid line, and the two minimum contours at 800 and 1000 K are drawn with short and long dashes. The top panel demonstrates that the temperature at equilibrium/saddle is highest under stoichiometric conditions and when enthalpy is highest, an unsurprising result.

The bottom two panels of Figure 12 show attractiveness of the one- and two-dimensional manifolds with the parameters α_1 and α_2 defined in eqs 4.1a and 4.1b. There are nine contours in the middle panel ranging from a minimum value of 100.0 to a maximum of 1700.0 in intervals of 200.0. The highest (upper right) and lowest (lower right and left) are plotted with thick solid lines and the value at 500.0 as dashed lines. The rest of the contours are plotted with thinner solid lines. These contours indicate that the surface defined in the middle panel consists of two ridges peaking at approximately $(\sigma,H) = (-0.6,7 \times 10^9)$ and $(0.6,7 \times 10^9)$ and moving down diagonally from there, with the higher ridge being the latter one.

The bottom panel has nine unevenly spaced contours to describe α_2 with the following values: 2.0, 3.0, 4.0, 15.0, 50.0, 100.0, 200.0, 300.0, 400.0. The first three sets of contours are plotted as thinner dashed lines, the next three with thicker dashed lines, and the highest three as solid lines. The bottom panel shows that the two-dimensional manifolds under lean conditions are not very attractive, with α_2 mostly near 2.0−4.0. Only under rich conditions do the two-dimensional manifolds become very attractive, and this does not depend in any significant manner on enthalpy.

Figure 13 describes the eigenvalue ratios near the saddlepoints for the flame systems. As noted above, the low-dimensional manifolds are submanifolds of a stable manifold of dimension 6 in all cases studied. The contour plots are over the same range of enthalpies and stoichiometry as those of Figure 12. The enthalpy in Figure 13 refers to the asymptotic average, $\bar{h}_\infty$. The top panel of Figure 13 shows α_1, and the bottom shows α_2. There are 12 contours. The lowest contour is 10.0 and is plotted as a solid line in the bottom left and right of the panel. There are 10 evenly space contours from 100.0 to 1000.0 in increments of 100.0, and the largest contour at 1500.0 is plotted as a thick solid line in the upper right, along with the second highest at 1000.0 with the same line type. The two contours at 100.0 and 200.0 are plotted as short and long dashes, respectively. The rest of the contours are plotted as thin solid lines. Once again, as in the case of α_1 for the chemical-kinetic system in Figure 12, there are two ridges in the plots, but the ridge in the rich portion of the plot is considerably higher than the one in the lean half. Although the one-dimensional manifolds near the

saddle for the flame are attractive throughout the parameter space shown in the top panel, they are considerably more attractive for rich flames.

As with the chemical-kinetic systems, the two-dimensional manifolds are considerably less attractive than the one-dimensional manifolds for the flames. In the bottom panel, the attractiveness of the submanifolds does not change qualitatively from the low-dimensional manifolds of chemical-kinetic systems, although they are less attractive.

V. Trajectories

A. Generating Flame Trajectories. Because the dynamical system of eq 3.1d is unstable and trajectories cannot be integrated in the usual manner, it is necessary to devise a different procedure to follow trajectories on the stable manifold of the saddlepoint. Equation 3.1d is written in the discrete form as:

$$\Delta y_k - F_k \Delta x_k = 0 \tag{5.1a}$$

An analogous version of these equations can be written in the time domain for the chemical-kinetic case of eqs 2.1a and 2.1b:

$$\Delta y_k - F_k \Delta t_k = 0 \tag{5.1b}$$

An orbit of the system is then found by finding the roots of a nonlinear system of equations, in a manner similar to what is done in the program Premix for the boundary value problem.[31] Such procedures are well-known in the literature, for example, being used to find rare events.[37]

For the flame trajectories generated here, a small spatial step size is chosen initially for eq 5.1a, usually 10^{-4} to 10^{-6} cm, and then is scaled geometrically with the spatial coordinate. This means that the step sizes in eqs 5.1a and 5.1b at a given spatial or temporal step are:

$$\Delta x_k = (\alpha_x)^k \Delta x_0, k = 0 \rightarrow n \tag{5.2a}$$

$$\Delta t_k = (\alpha_t)^k \Delta t_0, k = 0 \rightarrow n \tag{5.2b}$$

The α's in eqs 5.2a and 5.2b are usually between 1.05 and 1.25. Generally n is between 100 and 150. In one case below (Figure 16), the calculation was run at a much finer scale to compare with a premix result. The initial guess for the orbit is the dynamics of a linear system based on the eigenvectors of the Jacobian, which is described in section III.A. For the linear system, the initial trajectories are written as displacements from their values at the saddlepoint for the flame systems and the equilibrium point for the chemical-kinetic systems. These displacements are then propagated and transformed back to the original coordinate system:

$$\delta y_k(x) = \sum_{m=1}^{n_s} a_{km} R_{mk} e^{\gamma_m x} \tag{5.3a}$$

$$\delta y_k(x = 0) = y_{k0} - y_k^0 \tag{5.3b}$$

$$a_{km} = \sum_{i=1}^{n_s} L_{mi}^T \delta y_{i0} \tag{5.3c}$$

where n_s refers to the dimension of the stable manifold. Equation 5.3b describes the displacement of the initial conditions of the trajectory from the saddlepoint or equilibrium point, and eq 5.3c describes the expansion of these displacements in terms of the eigenvectors of the stable manifold. The discrete versions of these trajectories are used as initial guesses into the Newton−Raphson procedure used to solve eqs 5.1a and 5.1b. Equation 5.3a has

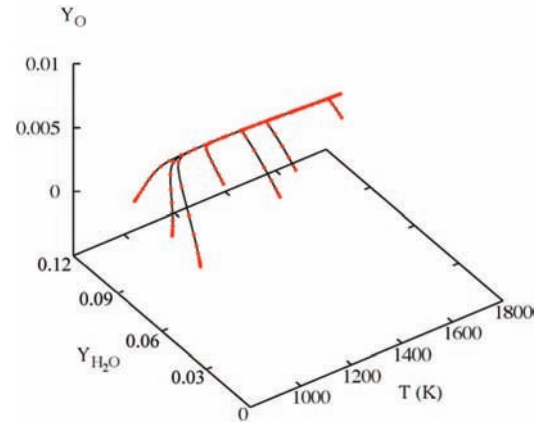

Figure 14. Seven trajectories for a chemical-kinetic system were generated by integrating them and are plotted with a solid line. These are compared to trajectories generated by the Newton−Raphson procedure outlined here, and these are plotted as a series of dots. These estimates lie right on top of the integrated versions. For the Newton−Raphson algorithm, $\Delta t_0 = 1.0 \times 10^{-5}$ s and $\alpha_t = 1.1$ (eq 5.2b). There are 100 steps for each trajectory with a total time of 1.38 s for each. The initial trajectory guesses for the Newton−Raphson [eqs 5.3] used the following γ's: −1.0, −600.0, −18 000, −36 000, −40 000, −100 000.

"x" as the independent coordinate, which is used for the flame dynamics. For the chemical-kinetic trajectories, "t" is the independent coordinate. The L's and R's refer to the left and right eigenvectors of the Jacobian of eq 2.4, which is diagonalized in the usual manner:[38]

$$\lambda = \mathbf{L}^T \mathbf{J} \mathbf{R} \tag{5.4}$$

It was found that better convergence could be obtained with starting guesses in eq 5.3a that had exponential factors, the γ's, that are different than the eigenvalues, the λ's, so these are used as adjustable parameters.

The step sizes and number of steps in eqs 5.2a and 5.2b are chosen so that there are several points near the saddlepoint at the end of the propagation of the initial linear system in eqs 5.3a−5.3c. Six initial conditions are fixed at $t = 0$ and $x = 0$, because the stable manifold is six-dimensional. Some care is necessary in applying the algorithm, and there are times when the algorithm does not converge or convergence is poor, and the parameters need to be adjusted.

This procedure is first tested on a chemical-kinetic system using eq 5.1b. For this case, it is possible to integrate trajectories using eqs 2.1a and 2.1b, because the system is stable. As noted in eq 5.1b, the independent coordinate in this case is time, and Δt takes the place of Δx in eq 5.1a. The time step sizes are described in the caption to Figure 14 where the results of a test are shown. The shortest chemical-kinetic time scales are not included in these trajectories, with the initial time step set to 10^{-5} s. This means that the fastest transients are not observed in the trajectories. There are seven trajectories shown in Figure 14, and the orbits found from a Newton−Raphson search are compared to the results of an integration of trajectories using the program LSODE.[39] The solid lines in Figure 14 are the results of the integration, and the dots result from the Newton−Raphson procedure. These two sets of results lie on top of each other.

B. Trajectory Examples. The procedure outlined in the previous subsection is now applied to a flame trajectory in Figure 15. Once again, six initial conditions are set at the beginning of the trajectory because the stable manifold is six-dimensional based on the number of negative eigenvalues at the saddlepoint,

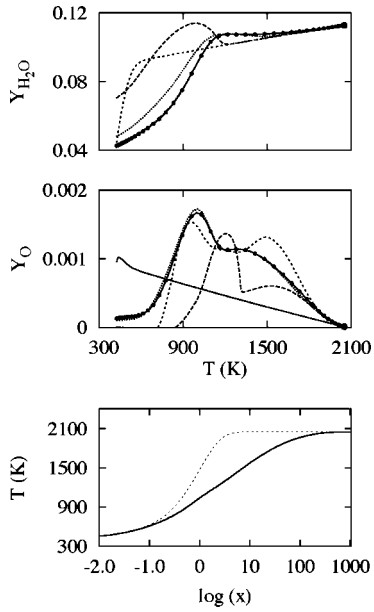

Figure 15. Two views of the convergence process are shown in the top two panels for the H_2O and O mass fractions. The bottom panel shows the initial and final temperature distribution as a function of the log of the spatial coordinate. The value of Δx_0 is 10^{-6} cm and $\alpha_x = 1.15$. There were 120 spatial steps used. The values of the γ's are -1.0, -50.0, -200.0, -400.0, -400.0, and -400.0.

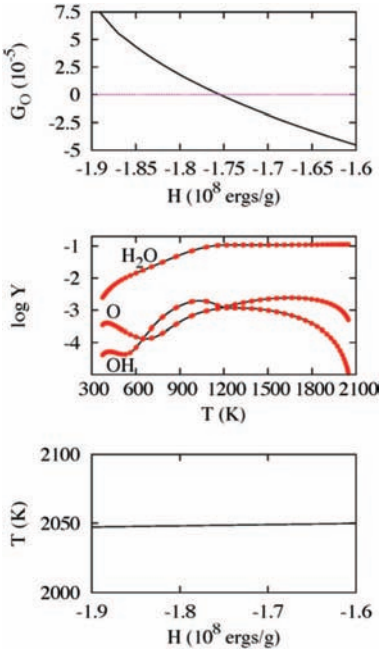

Figure 16. The top panel describes the calculation of a steady flame with the proper initial mass flux fractions. The middle panel compares the trajectory calculation with the steady flame calculated with premix, presented in Figure 2, and the bottom panel shows the asymptotic temperature for the set of calculations. The value of Δx_0 is 6×10^{-5} cm and $\alpha_x = 1.028$, with 450 spatial steps. The values of the γ's are -1.0, -50.0, -200.0, -400.0, -400.0, and -400.0.

as discussed above. The other 10 coordinates are allowed to relax in the 16-dimensional system. The finite-difference in eq 5.1a is accomplished by three-point central differences for all points except for the 10 coordinates at the beginning of the trajectory that are allowed to relax. Forward three-point differences are used for these. The Δy_k's at the end of the trajectory are calculated by backward three-point differences for all 16 coordinates.

The shorter dashed line in the top panel of Figure 15 is the initial orbit guess based on linear dynamics, the longer dashed line with a maximum near $T = 1000$ K is the first iteration, the dotted line is the third iteration, and the lighter line is the fourth iteration. The fully converged result is shown with a thick solid line. In the Y_O projection in the middle panel, the line types used for the top panel now show the initial orbit, and then the second through fourth iterations, with the solid thick line once again showing the converged trajectory. The bottom panel of Figure 15 shows the temperature of the initial orbit guess, and the solid line once again shows the fully converged result. The temperature results are plotted versus $\log(x)$, the spatial coordinate.

The trajectory shown in Figure 15 is for a system with the following constants (eqs 3.2a and 3.2b): $d_O = 0.0063$ and $d_{Ar} = 0.88$. The asymptotic enthalpy of the mixture is -1.755×10^8 ergs/g. Results for this system were presented in Figures 7 and 8. The values of the constants agree with those calculated from the results of the Premix code to at least 4 significant figures, but the asymptotic enthalpy from the premix code is slightly different, -1.607×10^8 ergs/g. We view this difference as within the errors of both calculations.

The calculation of the trajectory that matches the flame generated by the premix code is described in Figure 16. The initial values of the mass flux fractions of six species are fixed in the same manner as they are in the Premix code. In this case, the mole fraction of H_2 is set to 0.28, the mole fraction of O_2 to 0.09, and the mole fraction of Ar is set to 0.63. The rest of the mole fractions are set to zero. The mass fractions are then defined from these, and the mass flux fractions at the burner ($x = 0$) are set equal to the mass fractions (after the steady flame is solved, all mass fractions and mole fractions are nonzero at the burner, because of diffusion back toward the burner). The values of the mass flux fractions fix the constants. The temperature is set to 373.7 K.

After taking account of the constants and the fact that the mass flux fractions sum to 1.0, there are six independent mass flux fractions. Because the stable manifold is six-dimensional, only five of these are fixed at $x = 0$, all of the G's except G_O. These and the fixed temperature give the necessary six variables. A value of the asymptotic enthalpy leads to a trajectory using the algorithm outlined above. The mass flux fraction that is not fixed, G_O, relaxes to a final value that is nonzero for all values of the asymptotic enthalpy except those that define the steady flame with the correct values at the burner.

The top panel of Figure 16 shows a set of calculations of G_O for a set of systems with the two constants set to the values described above, and a series of asymptotic enthalpies. This curve crosses $G_O = 0$ at $H = -1.755 \times 10^8$ ergs/g, defining the proper steady flame. The middle panel compares the trajectory with the steady flame of Figure 2, and agreement is good. There are some small discrepancies not evident from the plot, but these are in species with small mass fractions, such as O-atom and OH. The asymptotic temperatures differ by about 2 K out of 2050 K. The bottom panel of Figure 16 shows how the asymptotic temperature varies with asymptotic enthalpy for the flame trajectories.

Figure 17 shows a set of 394 flame trajectories generated at the value of the asymptotic enthalpy established in Figure 16, with the same constants used there. The initial conditions for the trajectories were randomly sampled over a range of values fixed by the saddlepoint. The four trace species, O, OH, HO_2, and H_2O_2, are chosen to have mass flux fraction values (G's) that lie between 0.0 and 10.0 times their values at the saddlepoint. The mass flux fraction of H_2O is chosen between

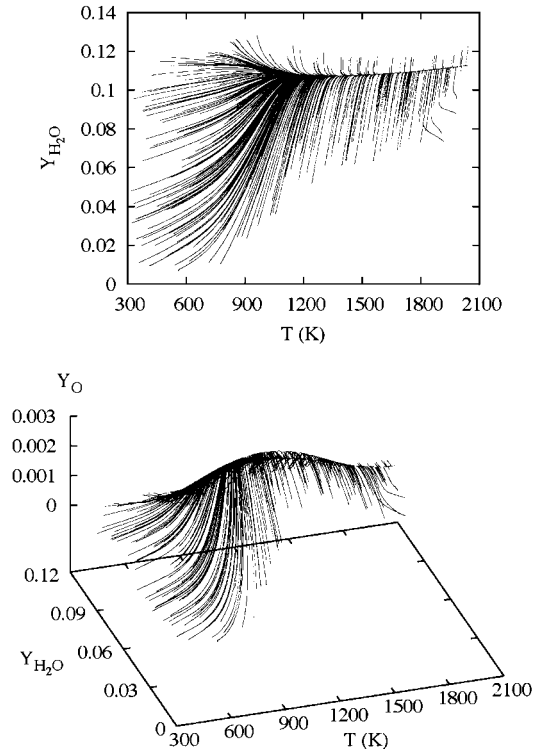

Figure 17. A set of 394 trajectories generated with the algorithm of section V.A. are shown here. These were generated from randomly selected initial conditions with the ranges described in the text. The top panel shows a two-dimensional projection, and the bottom panel shows a three-dimensional projection. The value of Δx_0 is 10^{-6} cm and $\alpha_x = 1.15$. There were 135 spatial steps used. The values of the γ's are -1.0, -50.0, -200.0, -400.0, -400.0, and -400.0.

zero and 1.2 times its value at the saddlepoint. The temperature is chosen to be between 0.15 of its value at the saddle and the actual value at the saddle, $T = 2050$ K. An initial sample of 449 trajectories led to 400 trajectories that converged. We expect that most of the trajectories that did not converge lay off the stable manifold, but it is difficult to state this with certainty in all cases. In addition, there were six trajectories that did not appear to be properly converged based on visual inspection, and these were also not included in Figure 17.

The trajectories in the top panel of Figure 17 indicate that there is an attractive one-dimensional manifold that starts near 1200 K and extends to the saddlepoint (see ref 5). This result is consistent with results near the saddlepoint. It was noted in section IV.A that the negative eigenvalues at the saddlepoint for this system are -0.0061, -2.3, -19.0, -22.7, -27.1, and -69.2, indicating that the one-dimensional manifold is highly attractive near equilibrium. It is also consistent with those of Figures 10 and 12 that show strong attractive properties for the one-dimensional submanifold of the stable manifold near the saddlepoint.

The bottom panel of Figure 17 gives a strong indication that there is an attractive two-dimensional manifold. This again is consistent with the dynamics near equilibrium where the eigenvalue ratio (eq 4.1b) is $-19.0/-2.3 = 8.3$, indicating a two-dimensional submanifold that is reasonably attractive near equilibrium.

C. Analysis of Trajectories. The trajectories generated in the previous section are now analyzed in more detail to ascertain how they compare to adiabatic isobaric chemical-kinetic trajectories and to make an assessment of the low-dimensional submanifolds for the stable manifold. The nature of the submanifolds will be studied in more detail in the subsequent publication,[5] where the submanifolds will be explicitly generated and will be used to compare the chemical kinetics with the flames.

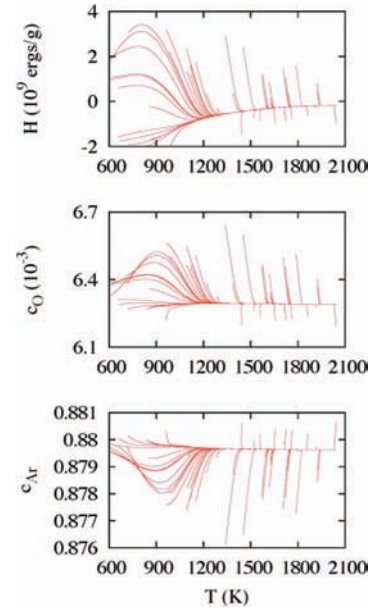

Figure 18. A series of plots studying a subset of the trajectories in Figure 17. The three quantities studied in the flame trajectories are constant for adiabatic, isobaric chemical kinetics.

A set of calculations is presented in Figure 18 for a subset of the trajectories of Figure 17, similar to the information presented in Figure 3 for a steady flame. The top panel shows the enthalpy of the mixture, and the next two panels show the chemical-kinetic constants c_O and c_{Ar} defined in eqs 2.2a and 2.2b. The ranges of the y-axes in the bottom two plots are much smaller than that of the top panel, an indication that the enthalpy, which is constant in the chemical-kinetic problem, varies to a much greater extent in the flame than the other two quantities that are constant for adiabatic, isobaric chemical kinetics. Another important feature of these plots is what happens at the larger spatial extents where a one-dimensional manifold was evident in the top panel of Figure 17. There is a much smaller range of enthalpies along the manifold and nearly constant values for the chemical-kinetic constants.

The analysis of trajectories is continued in Figure 19, which shows the difference between the mass flux fractions and mass fractions along the same trajectories as in Figure 18. These plots show two different species and indicate that the one-dimensional manifold is characterized by a lack of transport. Equation 2.5c defined the mass flux fractions, the G's, in terms of the mass fractions, diffusion velocity, mass flow rate, and density. The G's and Y's coincide when the diffusion velocity is small as compared to the mass flow rate, which is what happens on the one-dimensional manifold, suggesting the one-dimensional manifold describes dynamics that is chemical-kinetic in nature, rather than diffusive. These results suggest that there may not be significant differences between one-dimensional manifolds for the flame system and the analogous chemical-kinetic system, and this will be confirmed in the following Article.[5]

VI. Conclusion

This Article has studied the spatial dynamics of one-dimensional steady H_2/O_2 premixed flames. The approach is motivated by the results generated by the Chemkin code Premix

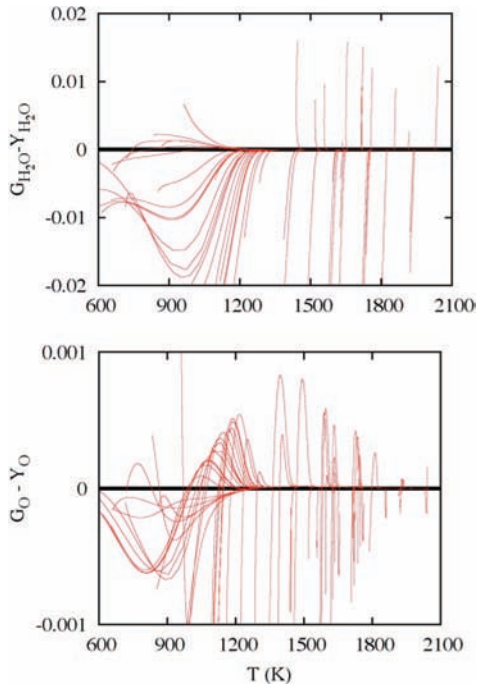

Figure 19. These plots demonstrate that along the one-dimensional manifold the *G*'s (mass flux fractions) and *Y*'s (mass fractions) are approximately equal. The thick line shows the zero line for their differences.

in Figures 4 and 6 that suggested there were low-dimensional manifolds in the dynamics of these systems, a result consistent with many years of studying the asymptotics of flames.

The spatial dynamics of steady flames was written as a dynamical system as outlined a number of years ago by Hirschfelder and Curtiss,[3] as well as Dixon-Lewis.[4] This formulation allows a more direct comparison between the temporal behavior of homogeneous chemical kinetics and the spatial dynamics of flames when this comparison is made in phase space where the difference in the independent variables (time vs space) is not important. It was shown that there are saddlepoints in the flame systems that correspond to the equilibrium points of adiabatic isobaric chemical kinetics, and although these flame systems are unstable, steady flames are trajectories on the stable manifolds of the saddlepoints. An important numerical result is that in almost all cases studied here, the dimension of the stable manifold of the flames matched the dimension of the corresponding adiabatic, isobaric chemical kinetics.

The eigenvalues of the Jacobian at the saddlepoint have been studied in detail (Figures 10 and 13), and it was shown that near the saddlepoint there is a separation of spatial scales on the stable manifold that leads to attractive submanifolds. The attractive submanifolds are equivalent to the low-dimensional manifolds of a typical adiabatic isobaric chemical-kinetic system, leading to the notion that standard techniques of finding low-dimensional manifolds can be utilized for the flames in the extended phase space studied here and in ref 5 and consistent with the results of ref 20.

To study the dynamics of the flame systems, it was necessary to devise methods for generating trajectories, because direct numerical integration cannot be accomplished due to the unstable nature of the systems. The methodology was laid out and several cases were studied in section V, including the reproduction of the flame generated previously using the Premix code in Figure 2. The behavior of ensembles of these trajectories gave strong evidence in Figure 17 that there are attractive one- and two-dimensional submanifolds of the stable manifold away from the saddlepoint, consistent with the local results of Figures 10–13. Figures 18 and 19 suggest that the relaxation that occurs along the one-dimensional manifold depends largely on chemical kinetics.

This Article lays the groundwork for what follows in the accompanying Article,[5] where low-dimensional manifolds are generated and there is a detailed comparison of the manifolds for chemical-kinetic systems and the flame systems. There will also be a comparison between two well-used methods for generating the manifolds. Because the methodology used here involves the study of an initial value problem, rather than a boundary value problem (Figures 7 and 8), this will allow a better comparison of the chemical-kinetic and flame manifolds.

Acknowledgment. This work was supported by the Office of Basic Energy Sciences, Division of Chemical Sciences, Geosciences, and Biosciences, U.S. Department of Energy, under Contract No. DE-AC02-06CH11357. A.S.T. was also supported by a Maria Goeppert Mayer Distinguished Scholarship at Argonne National Laboratory.

References and Notes

(1) For example: (a) Oran, E. S.; Boris, J. P. *Numerical Simulation of Reactive Flows*; Cambridge University Press: Cambridge, 2001. (b) Warnatz, J.; Maas, U.; Dibble, R. W. *Combustion*; Springer: New York, 2001. (c) Kee, R. J.; Coltrin, M. E.; Glarborg, P. *Chemical Reacting Flow: Theory and Practice*; Wiley-Interscience: New York, 2003.

(2) See, for example: (a) Westbrook, C. K., Ed. Modeling of Laminar Flame Propagation in Premixed Gases: A special issue of *Combust. Sci. Technol.* 1983. (b) Peters, N., Ed. Numerical Methods in Laminar Flame Propagation.

(3) For example: Hirschfelder, J. O.; Curtiss, C. F. *Adv. Chem. Phys.* **1961**, *3*, 59.

(4) For example: Dixon-Lewis, G. *Proc. R. Soc.* **1968**, *A307*, 111.

(5) Davis, M. J.; Tomlin, A. S. *J. Phys. Chem. A* **2008**, *112*, 7784.

(6) (a) Griffiths, J. F. *Prog. Energy Combust. Sci.* **1995**, *21*, 25. (b) Tomlin, A. S.; Turányi, T.; Pilling, M. J. *Comp. Chem. Kinet.* **1997**, *35*, 293. (c) Okino, M. S.; Mavrovouniotis, M. L. *Chem. Rev.* **1998**, *98*, 243.

(7) Fraser, S. J. *J. Chem. Phys.* **1988**, *88*, 4732.

(8) (a) Roussel, M. R.; Fraser, S. J. *J. Chem. Phys.* **1990**, *93*, 1072. (b) Roussel, M. R.; Fraser, S. J. *J. Chem. Phys.* **1991**, *94*, 7106. (c) Roussel, M. R.; Fraser, S. J. *J. Phys. Chem.* **1991**, *95*, 8762. (d) Roussel, M. R.; Fraser, S. J. *J. Phys. Chem.* **1993**, *97*, 8316. (e) Roussel, M. R.; Fraser, S. J. *J. Phys. Chem.* **1994**, *98*, 5174. (f) Fraser, S. J.; Roussel, M. R. *Can. J. Chem.* **1994**, *72*, 800. (g) Fraser, S. J. *J. Chem. Phys.* **1998**, *109*, 411.

(9) (a) Nguyen, A. H.; Fraser, S. J. *J. Chem. Phys.* **1989**, *91*, 186. (b) Roussel, M. R. *J. Math. Chem.* **1997**, *21*, 385. (c) Roussel, M. R.; Fraser, S. J. *Chaos* **2001**, *11*, 196.

(10) Roussel, M. R. A Rigorous Approach to Steady-State Kinetics Applied to Simple Enzyme Mechanisms. Ph.D. Thesis, University of Toronto, 1994.

(11) (a) Maas, U.; Pope, S. B. *Combust. Flame* **1992**, *88*, 239. (b) Maas, U.; Pope, S. B. *Proc. Combust. Inst.* **1992**, *28*, 103.

(12) Maas, U.; Pope, S. B. *Proc. Combust. Inst.* **1994**, *25*, 1349.

(13) (a) Lam, S. H.; Goussis, D. A. *Int. J. Chem. Kinet.* **1994**, *26*, 461. For recent developments and important applications, see, for example: (b) Valorani, M.; Najm, H. N.; Goussis, D. A. *Combust. Flame* **2003**, *134*, 35, and references cited therein.

(14) Yannacopoulos, A. N.; Tomlin, A. S.; Brindley, J.; Merkin, J. H.; Pilling, M. J. *Physica D* **1994**, *83*, 421.

(15) Hdjinicolaou, M.; Goussis, D. A. *SIAM J. Sci. Comput.* **1999**, *20*, 781.

(16) Skodje, R. T.; Davis, M. J. *J. Phys. Chem. A* **2001**, *105*, 10356.

(17) Davis, M. J.; Skodje, R. T. *J. Chem. Phys.* **1999**, *111*, 859.

(18) Nafe, J.; Maas, U. *Combust. Theory Modell.* **2002**, *6*, 697.

(19) Singh, S.; Powers, J. M.; Paolucci, S. *J. Chem. Phys.* **2002**, *117*, 1482.

(20) Bongers, H.; Van Oijen, J. A.; De Goey, L. P. H. *Proc. Combust. Inst.* **2002**, *29*, 1371.

(21) Goussis, D. A.; Valorani, M.; Creta, F.; Najm, H. N. *Prog. Comp. Fluid Dyn.* **2005**, *5*, 316.

(22) Ren, Z. Y.; Pope, S. B.; Vladimirsky, A.; Guckenheimer, J. M. *J. Chem. Phys.* **2006**, *124*, 11411.

(23) Ren, Z. Y.; Pope, S. B. *Combust. Flame* **2006**, *147*, 243.

(24) (a) Davis, M. J. *J. Phys. Chem. A* **2006**, *110*, 5235. (b) Davis, M. J. *J. Phys. Chem. A* **2006**, *110*, 5257.

(25) Roussel, M. R.; Tang, T. *J. Chem. Phys.* **2006**, *125*, 214103.

(26) Bykov, V.; Maas, U. *Combust. Theory Modell.* **2007**, *11*, 839.

(27) Perko, L. *Differential Equations and Dynamical Systems*; Springer-Verlag: New York, NY, 1996.

(28) Turányi, T.; Tomlin, A. S.; Pilling, M. J. *J. Phys. Chem.* **1993**, *97*, 163.

(29) Lam, S. H. *Combust. Sci. Technol.* **2007**, *179*, 767.

(30) Smooke, M. D. *J. Comput. Phys.* **1982**, *48*, 72.

(31) Kee, R. J.; Grcar, J. F.; Smooke, M. D.; Miller, J. A. A Fortran Program for Modeling Steady Laminar One-Dimensional Flames, SAND85-8240, Sandia National Laboratories, 1985.

(32) Davis, M. J.; Zagaris, A.; Kaper, T. J.; Tomlin, A. S., to be submitted.

(33) O Conaire, M.; Curran, H. J.; Simmie, J. M.; Pitz, W. J.; Westbrook, C. K. *Int. J. Chem. Kinet.* **2004**, *36*, 603.

(34) Krauskopf, B.; Osinga, H. M.; Doedel, E. J.; Henderson, M. E.; Guckenheimer, J.; Vladmirsky, A.; Dellnitz, M.; Junge, O. *Int. J. Bifurfaction Chaos* **2005**, *15*, 763.

(35) Lowe, R.; Tomlin, A. *Atoms. Environ.* **2000**, *34*, 2425. Tomlin, A. S.; Whitehouse, L.; Lowe, R.; Pilling, M. J. *Faraday Disc.* **2001**, *120*, 125.

(36) See, for example: Seydel, R. *From Equilibrium to Chaos: Practical Bifurcation and Stability Analysis*; Elsevier: New York, NY, 1988.

(37) For example: Gillilan, R. E.; Wilson, K. R. *J. Chem. Phys.* **1992**, *97*, 1757.

(38) For example: Golub, G. H.; Van Loan, C. F. *Matrix Computations*; Johns Hopkins University Press: Baltimore, MD, 1996.

(39) Hindmarsh, A. C. In *Scientific Computing*; Stepleman, R. S., et al., Eds.; North-Holland: Amsterdam, 1983; p 55.

JP801367X